Navigation-Supported Diagnosis of the Substantia Nigra by Matching Midbrain Sonography and MRI

Zein Salah[a,c], David Weise[b], Bernhard Preim[c], Joseph Classen[b], and Georg Rose[a]

[a]Department of Electronics, Signal Processing and Communication Technology, University of Magdeburg, Germany;
[b]Department of Neurology, University of Leipzig, Germany;
[c]Department of Simulation and Graphics, University of Magdeburg, Germany

ABSTRACT

Transcranial sonography (TCS) is a well-established neuroimaging technique that allows for visualizing several brainstem structures, including the substantia nigra, and helps for the diagnosis and differential diagnosis of various movement disorders, especially in Parkinsonian syndromes. However, proximate brainstem anatomy can hardly be recognized due to the limited image quality of B-scans. In this paper, a visualization system for the diagnosis of the substantia nigra is presented, which utilizes neuronavigated TCS to reconstruct tomographical slices from registered MRI datasets and visualizes them simultaneously with corresponding TCS planes in real-time. To generate MRI tomographical slices, the tracking data of the calibrated ultrasound probe are passed to an optimized slicing algorithm, which computes cross sections at arbitrary positions and orientations from the registered MRI dataset. The extracted MRI cross sections are finally fused with the region of interest from the ultrasound image. The system allows for the computation and visualization of slices at a near real-time rate. Primary tests of the system show an added value to the pure sonographic imaging. The system also allows for reconstructing volumetric (3D) ultrasonic data of the region of interest, and thus contributes to enhancing the diagnostic yield of midbrain sonography.

Keywords: Transcranial sonography, MRI, Freehand ultrasound, Visualization, Substantia nigra

1. INTRODUCTION

Parkinson's disease (PD) is characterized by degeneration of dopaminergic neurons in the substantia nigra (SN, pars compacta). The diagnosis is classically made clinically based on the presence of the cardinal motor symptoms of the disease. However, establishing the diagnosis in the early phase is often difficult because clinical presentation often resembles other neurodegenerative diseases. Nuclear neuroimaging studies can be helpful in making a diagnosis of PD, but access is limited. Transcranial sonography (TCS) is a well-established, safe, easily applicable and low-cost neuroimaging technique that allows for visualizing several brainstem structures including the SN. It may be useful for the diagnosis and differential diagnosis of various movement disorders.[1] Using TCS, an echogenic area can be detected in the midbrain at the anatomical location of the SN and quantified planimetrically. Abnormal spatial extension of the echogenic SN size is a characteristic finding in PD and is regarded as a potential structural marker that may signal degeneration of dopaminergic nigrostriatal projection neurons.[2,3]

Reliability and specificity of echogenic SN area expansion is limited, as this structural marker is also found in other atypical parkinsonian disorders[4] and in up to 10% of healthy individuals.[5] Furthermore, accurate assessment of the borders of the echogenic SN in the axial plane is often difficult. Moreover, degeneration of the dopaminergic neurons in the SN in the course of the disease usually starts in the caudal part of the SN, whereas the planar size usually is measured in the more rostral portion of the SN. Hence, subtle changes in the echogenicity of the SN early in the degeneration process may be detected more easily by assessment of the 3D extension of the echogenic SN. In this context, a freehand ultrasound system can be adapted. Freehand 3D ultrasound systems

Further author information:
Zein Salah, E-mail: zein.salah@ovgu.de, Telephone: +49 391 6718781

gained an increasing interest in the last two decades. These systems utilize tracking technology to record the position and orientation data of acquired B-scan images in the frame of a global coordinate system, which in turn allows for reconstructing 3D volumes of the scanned regions.[6–8]

Assessment of the echogenic SN volume might improve the sensitivity of detecting PD at an early stage, and enhance specificity in the differential diagnosis of the disease. Furthermore, it should be theoretically possible to spatially monitor disease progression. However, the quality of TCS images does not allow for investigating neighboring relevant midbrain structures, which are on the other hand clearly depicted in MRI data. In this paper, we introduce a navigation-assisted system for the diagnosis of the substantia nigra. The system utilizes tracking data to reconstruct tomographical MRI* slices and to match them with the corresponding ultrasound images.

A crucial step in freehand ultrasound systems, from a technical point of view, is *probe calibration*. Principally, a targeted position, e.g., a point, is scanned from different positions and orientations and its locations are marked in the B-scan image. An iterative optimization technique is then used to solve for the calibration that matches positions in the 3D space with corresponding positions in B-scans. *Point phantoms* can take the form of a cross-wire[9] or a stylus.[10] Prager et al.[11] introduced the *single-wall phantom*, where a plane is scanned instead of a point. The scanned plane might be the bottom of the water bath or a plexiglass board.[12] A purposely built phantom, the *Cambridge phantom*, has been introduced to minimize inaccuracies due to beam thickness during scanning a single-wall phantom at oblique angles.[11] Lange et al.[13] solve for the calibration transform by scanning a phantom of known geometry and rigidly registering a virtual model of the phantom to the B-scan images.

Freehand ultrasound imaging allows for reconstructing B-scans into a regular voxel array, which allows for using conventional 3D visualization and data analysis techniques like slicing, surface rendering, volume rendering, and segmentation procedures. Rohling et al.[14] provided a comparison of 3D ultrasound reconstruction techniques. However, some methods allow for performing fast volumetric measurements directly from the B-scans,[15] or incrementally visualizing the volume during the scan process.[16] Barrat et al.[17] used a calibrated tracked ultrasound system within a bone registration scheme.

2. METHODS

2.1 System Setup Overview

The setup of our system, depicted in Figure 1, consists in the main part of a visualization module running on the control PC. B-scan images acquired by the ultrasound device (Siemens Acuson Anatares, Erlangen, Germany) are transmitted via a frame grabber. The ultrasound probe is spatially tracked using an optical infrared tracking camera (NDI Polaris). For this purpose, a rigid body marker is mounted on the probe. The tracking system provides, for each visible marker, the position and orientation data in the form of a transform between the marker coordinate system and that of the tracking camera. To compensate for patient movement, we configure the system to provide all transforms with respect to a reference marker that is fixed to special eyeglasses or a headband worn by the patient during the examination. The system includes modules for ultrasound probe to tracker calibration, patient to data registration, slicing, and overlaid visualization. These modules are described in the subsequent sections.

2.2 Ultrasound Probe Calibration

In a first step, a probe calibration is performed to compute the position and orientation of the B-Scan image with respect to the probe rigid body marker coordinate system, as depicted in Figure 2a. We adapted the method presented by Prager et al.,[11] which depends on scanning a single wall phantom in a water bath, thus generating a line in each ultrasound image. Lines, which are detected automatically in the ultrasound images, correspond to the same physical plane, so an optimization algorithm solves a system of independent equations to solve for unknowns (for details, please see Prager et al.[11]).

For more accurate results, we perform the calibration using a Cambridge phantom.[6,11] However, we modified the design of the Cambridge phantom, as shown in Figure 2b, to better allow for calibrating curvilinear ultrasound

*Technically, CT data can also be used, as Figure 3b shows.

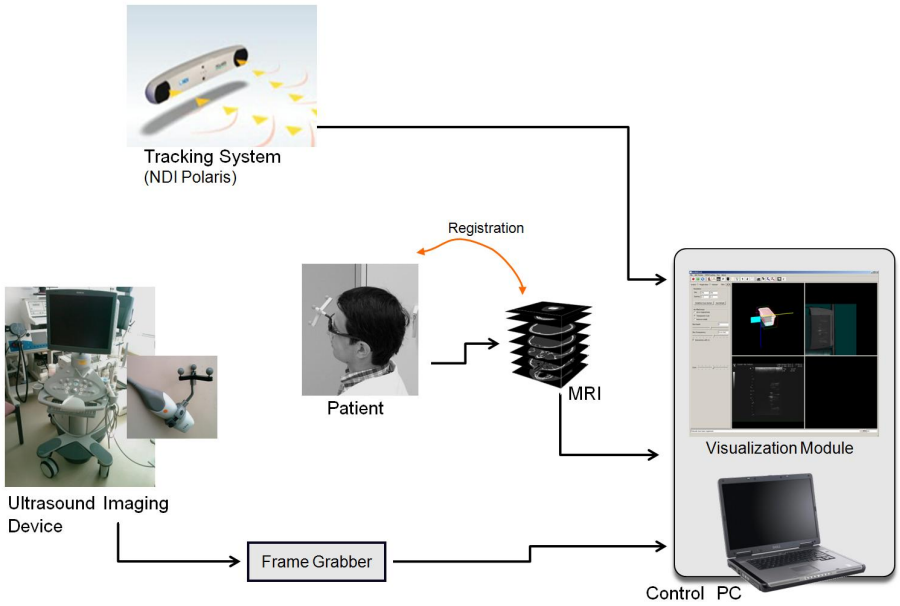

Figure 1. Setup of the ultrasound-MRI visualization system.

probes and scanning at a wider range of depths. The phantom is scanned in a water bath and the ultrasound probe is fixed in the upper part so that the scanned bar, marked with the arrow, lies exactly in the center of the ultrasound beam. The upper part slides up and down onto the lower bar and rolls from side to side. Since the upper edge of the bar is exactly aligned with the centers of the two wheels, it remains at a constant height above the floor of the water bath. Thus, the scanned lines in the ultrasound images lie in a virtual plane. To resemble the speed of sound in average human tissue, water temperature should be maintained at 50°C during the calibration process.

For the implementation of the calibration step we relied on the StradWin[†] software. The resulting calibration transformation T_{calib} remains valid as long as the rigid body marker is not moved relative to the US probe. During this step, temporal calibration is also performed to estimate the image lag mainly caused by the frame grabber.

The results of the calibration process are:

- The offset ($x-$ and $y-$coordinate of the upper left corner), width and height (in pixels) of a region of interest from the video stream of the ultrasound device, defining a cropped B-scan image.
- A transformation T_{calib} from the corner of cropped ultrasound image to the coordinate system of the tracking marker.
- $x-$ and $y-$scalings of the cropped ultrasound image (in mm/pixel).
- Image lag.

2.3 Registration

To create correct correspondences between the patient and the scanned dataset, a paired-point rigid registration scheme is employed. In essence, a set of landmark points is interactively selected from the patient dataset (usually, MRI). These landmarks are chosen such that they represent clearly-definable positions on the outer skin of the head. Absolute 3D positions in the dataset coordinate system are calculated considering landmark voxel coordinates and image spacing. The set of corresponding point positions in the patient coordinate system is defined by requiring the user to probe each landmark with a tracked pointer. Landmark points are rendered

[†]http://mi.eng.cam.ac.uk/rwp/stradwin/

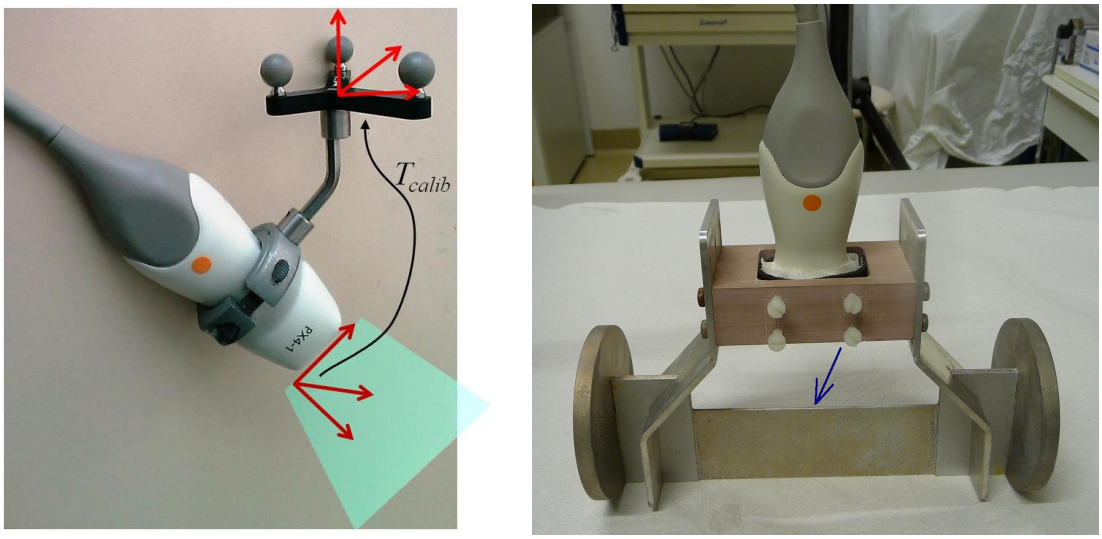

(a) (b)

Figure 2. a) Probe calibration transformation. b) Modified Cambridge phantom.

within a 3D overview of the patient face (see the upper left widget of Figure 4) to guide the user by probing points.

Finally, a registration transform T_{reg} between the two correspondence point sets is calculated based on the method presented by Horn.[18] Principally, three landmark points are sufficient to calculate the registration transform. However, we use more points to allow for a more accurate registration and minimize the effect of human error during selecting points and probing for position. Examples for potential landmarks are tip and root of nose and the two tragus tips.

2.4 Overlaid Ultrasound/Slice Visualization

A central functionality of the visualization module is the fusion of ultrasound images with on-the-fly reconstructed corresponding MRI tomographical cross sections. To this end, we adapt an optimized slicing algorithm to compute the cross sections at the desired position and orientation. Starting at the upper left corner, the algorithm applies an incremental approach to compute, for each pixel location in the cross section plane, the corresponding 3D location in the scanned data coordinate system, and evaluates the final pixel intensity using tri-linear interpolation. Thereby, pixel sizes of the planar slice to be computed and volumetric data (spacings) are taken into account to compute the (physical) position values (for details, see Salah et al.[19]). For the slicing algorithm, position and orientation are extracted from the transform T_{slicer}, which is computed as:

$$T_{slicer} = T_{reg}^{-1}.T_{probe-marker}.T_{calib} \tag{1}$$

where $T_{probe-marker}$ is the transform of the rigid body marker attached to the US probe.

Finally, two rectangles are textured with the cropped ultrasound image and the generated cross section image, respectively, considering image dimensions and spacings. The two rectangles are overlaid using alpha blending, applying an orthogonal projection matrix. The blending factor can be controlled to produce the desired view. At this step, windowing can be applied to the MRI cross section to focus on specific tissue or structures.

3. IMPLEMENTATION AND RESULTS

For the development and first experiments, we relied on phantom models. As shown in Figure 3a, a phantom consists primarily of a thin-walled plastic beaker. Air-filled pipes of an outer radius of 4 mm and inner radius

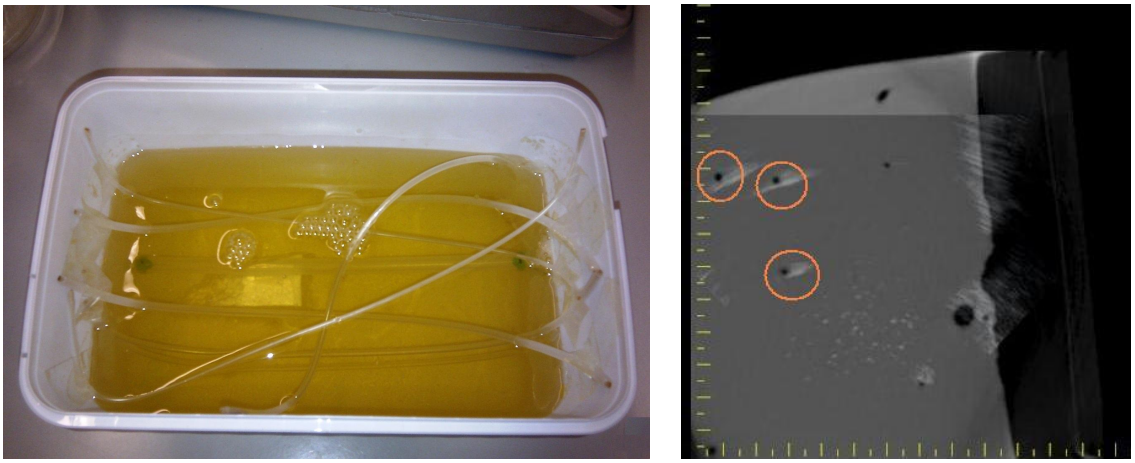

(a) (b)

Figure 3. Gelatine phantom: a) Construction of the phantom. b) Overlaid display of an ultrasound image with a computed CT cross section.

of 2 mm are spread in the beaker in different patterns. The beaker is then filled with a gelatine-based hydrogel. The hydrogel is prepared by desolving gelatine powder (20%) and propanol (2%) in hot water (78%). Mixing continues for about 15 minutes. Finally, the phantom is left to cool down to room temperature for a few hours. Afterwards, it is kept in a refrigerator.

The visualization module has been implemented with C++ (Microsoft Visual Studio 2005). Rendering was performed using OpenGL, and the GUI was implemented using the Qt library. For the current implementation, we utilized the StradWin software to perform the probe calibration step.

Figure 3b shows a blended view of an ultrasound image of the gelatine phantom with an on-the-fly computed cross section from the CT dataset. The regions marked with the circles demonstrate how the two images align. The black dots represent the air-filled space in the pipes from the CT slice, while the white spots result from reflection of ultrasound on the outer walls of the pipes.

Figure 4 shows a snapshot of the described visualization system. In addition to the live ultrasound video stream (lower left widget), the main module provides two viewing widgets. The upper left widget shows a 3D overview of the patient under examination. A 3D model of the face is reconstructed from the scanned MRI data using the Marching Cubes algorithm. This view allows for visually verifying the tracking, calibration, and registration procedures. Moreover, the currently generated MRI cross section is also rendered in the correct location relative to the extracted face model. This slice view can also be replaced by the acquired ultrasound image. For the registration, 4-6 correspondence point pairs were defined.

The upper right widget provides a view of the required region from the ultrasound image, overlaid on the reconstructed MRI tomographical slice. The blending factor can be controlled to produce the desired view. In this regard, the slicing algorithm allows for a computation rate of about 30 fps, which keeps up with the ultrasound video frame rate of 25 fps (depending on the used frame grabber). However, the image digitalization process within the frame grabber causes an image lag of about 100 ms, which is compensated for during the overlaying process.

In Figure 5, several transcranial sonography images with corresponding MRI images are shown, where different midbrain structures are depicted. The left images show 3D views and the middle ones show the original ultrasound images. The right images show the overlaid views of ultrasound images with tomographical slices from MRI. We slightly amplified the red channel of the MRI slices to facilitate differentiation from the blended ultrasound images.

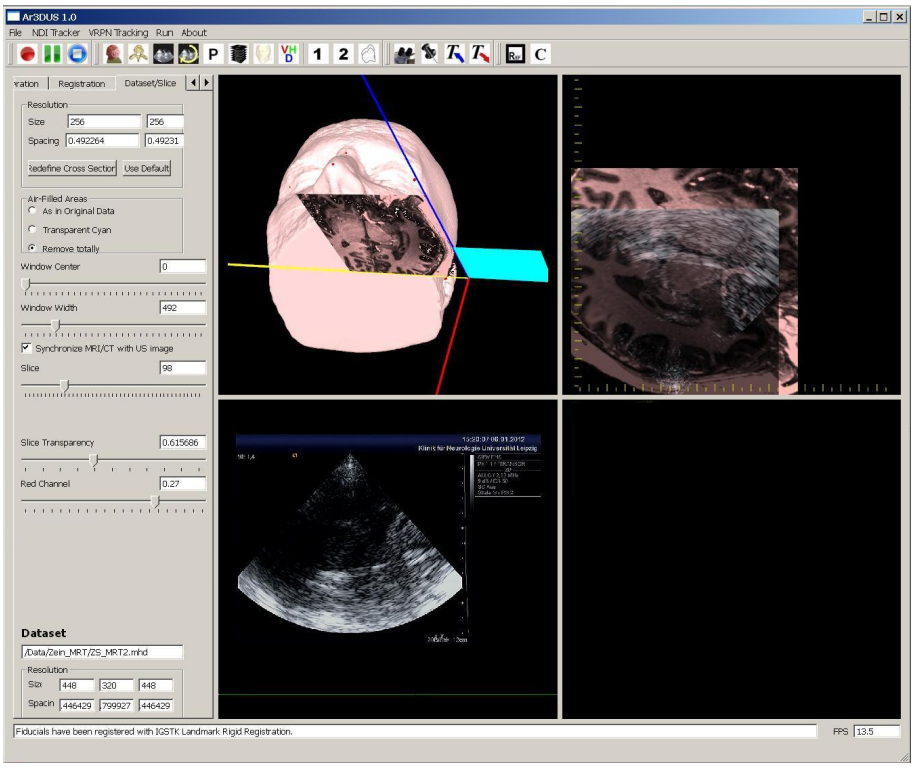

Figure 4. Snapshot of the visualization module.

4. DISCUSSION AND CONCLUSIONS

Most freehand 3D ultrasound systems aim, in the main part, at generating a volumetric dataset of the recorded B-scan images. In this paper, we also utilize the tracking system to augment the ultrasound images with corresponding cross-sectional tomographical slices of another modality. The advantage is to directly fuse anatomical structures that can be depicted with one modality with the proximate structures that are better (or only) visible in other modalities, like the substantia nigra in our case application. We are not aware of other systems treating the same issue.

The system presented in this paper utilizes neuronavigated TCS to reconstruct MRI planes from a registered dataset and visualize them simultaneously with TCS planes in real-time. The essential components of the system (tracking, calibration, registration, and rendering) have been described.

The goal thereby is to enhance the diagnostic yield of midbrain sonography. Using neuronavigated TCS, it would become possible to calculate and visualize the volume of the echogenic SN, and the system will provide a basis for detecting extensions of SN echogenicity in Parkinson's disease.

ACKNOWLEDGMENTS

This work is funded by the German Ministry of Education and Science (BMBF) within the ViERforES project (no. 01IM10002B). We also thank Daniel Stucht from the Department of Biomedical Magnetic Resonance for his support by the preparation of MRI data.

REFERENCES

[1] Berg, D., Godau, J., and Walter, U., "Transcranial Sonography in Movement Disorders," *The Lancet Neurology* **7**(11), 1044–1055 (2008).

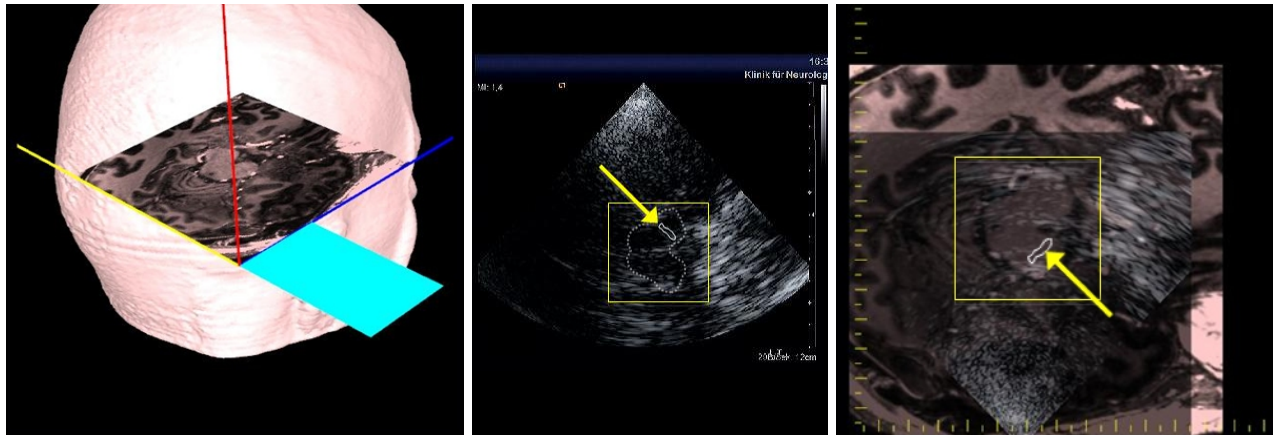

(a)

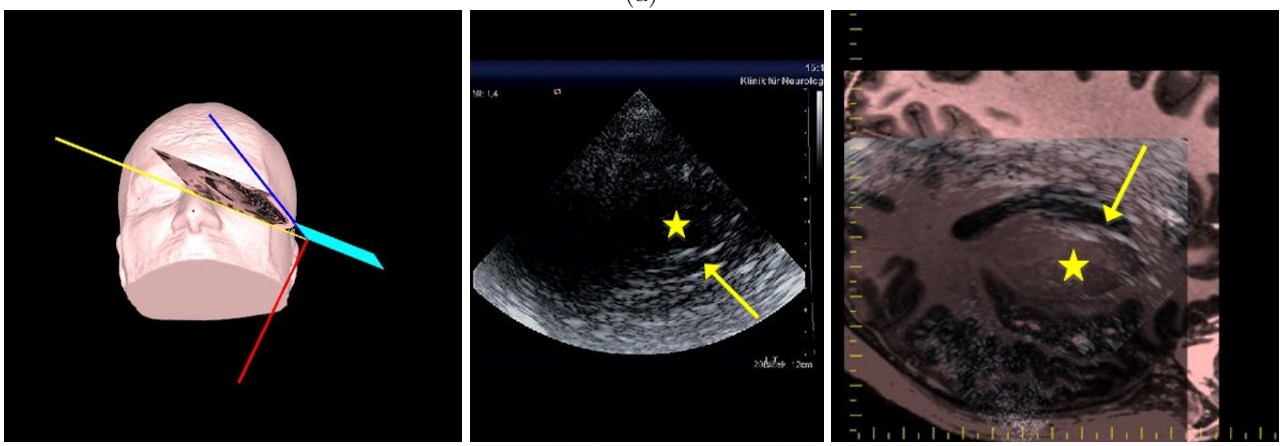

(b)

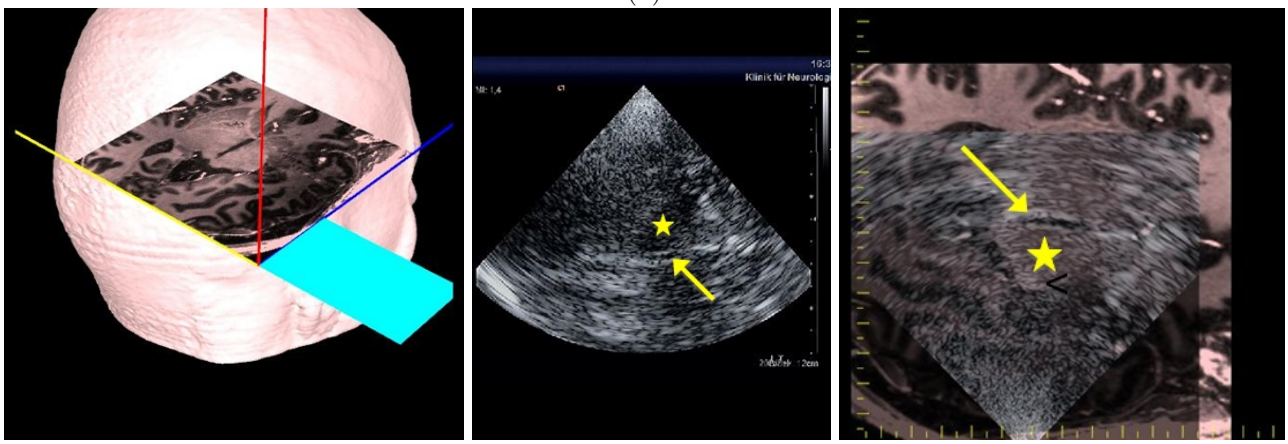

(c)

Figure 5. Corresponding transcranial sonography and MRI image showing different midbrain structures: (a) The rectangle defines a region of interest, the dotted line delineates the Mesencephalon, the solid line and the arrow mark the substantia nigra. (b) Lateral ventricle. (c) The arrow defines the third ventricle and the asterisk marks the thalamus.

[2] Weise, D., Lorenz, R., Schliesser, M., Schirbel, A., Reiners, K., and Classen, J., "Substantia Nigra Echogenicity: A Structural Correlate of Functional Impairment of the Dopaminergic Striatal Projection in Parkinson's Disease," *Movement Disorders* **24**(11), 1669–1675 (2009).

[3] Behnke, S., Schroeder, U., Dillmann, U., Buchholz, H., Schreckenberger, M., Fuss, G., Reith, W., Berg, D., and Krick, C., "Hyperechogenicity of the Substantia Nigra in Healthy Controls is Related to MRI Changes and to Neuronal Loss as Determined by F-Dopa PET," *Neuroimage* **47**(4), 1237–1243 (2009).

[4] Walter, U., Dressler, D., Probst, T., Wolters, A., Abu-Mugheisib, M., Wittstock, M., and Benecke, R., "Transcranial Brain Sonography Findings in Discriminating Between Parkinsonism and Idiopathic Parkinson Disease," *Archieves of Neurology* **64**(11), 1635–1640 (2007).

[5] Berg, D., Becker, G., Zeiler, B., Tucha, O., Hofmann, E., Preier, M., Benz, P., Jost, W., Reiners, K., and Lange, K., "Vulnerability of the Nigrostriatal System as Detected by Transcranial Ultrasound," *Neurology* **53**(5), 1026–1031 (1999).

[6] Treece, G., Gee, A., Prager, R., Cash, C., and Berman, L., "High Definition Freehand 3D Ultrasound," *Ultrasound in Medicine and Biology* **29**(4), 529–546 (2003).

[7] Pratikakis, I., Barillot, C., and Darnault, P., "Towards Free-Hand 3-D Ultrasound," Tech. Rep. No.4399, INIRIA (September 2001).

[8] Boctor, E., Viswanathan, A., Pieper, S., Choti, M., Taylor, R., Kikinis, R., and Fichtinger, G., "CISUS: An Integrated 3D Ultrasound System for IGT using a Modular Tracking API," *Proc. SPIE* **5367**, 247–256 (2004).

[9] Barry, C., Allott, C., John, N., Mellor, P., Arundel, P., Thomson, D., and Waterton, J., "Three-Dimensional Freehand Ultrasound: Image Reconstruction and Volume Analysis," *Ultrasound in Medicine Biology* **23**(8), 1209–1224 (1997).

[10] Hsu, P., Prager, R., Houghton, N., Gee, A., and Treece, G., "Accurate Fiducial Location for Freehand 3D Ultrasound Calibration," *Proc. SPIE* **6513** (2007).

[11] Prager, R., Rohling, R., Gee, A., and Berman, L., "Rapid Calibration for 3D Freehand Ultrasound," *Ultrasound in Medicine and Biology* **24**(6), 855–869 (1998).

[12] Rousseau, F., Hellier, P., and Barillot, C., "Confhusius: A Robust and Fully Automatic Calibration Method for 3D Freehand Ultrasound," *Medical Image Analysis* **9**(1), 25–38 (2005).

[13] Lange, T., Kraft, S., Eulenstein, S., Lamecker, H., and Schlag, P., "Automatic Calibration of 3D Ultrasound Probes," *Proc. Workshop Bildverarbeitung für die Medizin*, 169–173 (2011).

[14] Rohling, R., Gee, A., and Berman, L., "A Comparison of Freehand Three-Dimensional Ultrasound Reconstruction Techniques," *Medical Image Analysis* **3**(4), 339–359 (1999).

[15] Treece, G., Prager, R., Gee, A., and Berman, L., "Fast Surface and Volume Estimation from Non-Parallel Cross-Sections for Freehand Three-Dimensional Ultrasound," *Medical Image Analysis* **3**(2), 141–173 (1999).

[16] Dai, Y., Tian, J., Dong, D., Yan, G., and Zheng, H., "Real-Time Visualized Freehand 3D Ultrasound Reconstruction Based on GPU," *IEEE Transactions on Information Technology in Biomedicine* **14**(6), 1338–1345 (2010).

[17] Barratt, D., Penney, G., Chan, C., Slomczykowski, M., Carter, T., Edwards, P., and Hawkes, D., "Self-Calibrating 3D-Ultrasound-Based Bone Registration for Minimally Invasive Orthopedic Surgery," *IEEE Transactions on Medical Imaging* **25**(3), 312–323 (2006).

[18] Horn, B., "Closed-Form Solution of Absolute Orientation using Unit Quaternions," *Journal of the Optical Society of America* **4**(4), 629–642 (1987).

[19] Salah, Z., Preim, B., and Rose, G., "Prototype of an AR-Based System for Enhanced Visualization Functionality in Navigated Neurosurgery," *Proc. 7. Fachtagung zur Virtual Reality, Digitales Engineering und virtuelle Techniken*, 329–336 (2010).